All the data are consistent with the interpretation that the excitation function to a given vibration level of the $A\,^3\Sigma_u^+$ state increases linearly with energy for about 3 V above threshold. The curvature in i_s near threshold would then result from continuous excitation of new vibrational levels as they become energetically possible. However, certain reservations should be expressed about further, quantitative interpretation of the data near threshold. The position and, hence, the slope of the straight-line segments are somewhat subjective. This leads to uncertainty in the threshold energy for excitation of a given vibrational level. It is hoped that more refined experiments in the future may allow us to obtain more quantitative results in this region near threshold.

ACKNOWLEDGMENTS

I am indebted to Dr. Eric Kay and Dr. Erich Sawatzky for many helpful suggestions and discussions. I am also grateful to Mr. Curtis Erickson who skillfully built the tubes used in the present experiment.

THE JOURNAL OF CHEMICAL PHYSICS VOLUME 43, NUMBER 3 1 AUGUST 1965

Rigid Disks at High Density

FRANK H. STILLINGER, JR., ZEVI W. SALSBURG,* AND ROBERT L. KORNEGAY
Bell Telephone Laboratories, Incorporated, Murray Hill, New Jersey

(Received 31 March 1965)

A technique is developed for estimating the rigid-disk partition function near close packing, by evaluating the specific free-energy contributions from correlated motion of larger and larger sets of contiguous particles. In terms of the reduced density $\theta = A_0/A$ (A_0 is the close-packed value of the closed system's area A), the theory leads to an asymptotic series in the limit $\theta \to 1$ for the Helmholtz free energy per particle, divided by kT, of the form:

$$F/NkT \sim 2\ln(\lambda/a) - 2\ln(\theta^{-1}-1) + C + D(\theta^{-1}-1) + \ldots,$$

in which C and D are appropriate numerical constants, λ is the mean thermal de Broglie wavelength, and a the disk diameter. It is shown that lattice defects cannot contribute to the above asymptotic series. The constant C is expressed as an infinite series whose leading term is the single-particle free area result $[-\ln(\sqrt{3}/2)]$, and whose successive terms account for high-compression cooperative motions involving ascending numbers of particles. An approximate value for C is obtained by computing all contributions for four or fewer correlated disks, with a resulting slight decrease below the free area value. The calculated C may be utilized along with machine-computed rigid-disk pressures on both fluid and solid isotherm branches to locate accurately the first-order phase transition by means of a Maxwell double tangent construction.

Some concluding remarks are directed to application of the present method to rigid spheres in three dimensions, where the high density stable crystal structure could be established by suitable extension of the present formalism.

I. INTRODUCTION

ONE of the most useful adjuncts, developed in recent years, to the analytic theory of the classical many-body problem is high-speed electronic computer simulation of both equilibrium and irreversible behavior. With currently available computing speeds and memory capacities, the two-dimensional rigid-disk system has particular simplification advantages without a sacrifice of the interesting phase transition property.[1] Unfortunately, however, in the equilibrium regime even electronic computers are incapable of evaluating canonical partition functions (i.e., Helmholtz free energies) directly, but must be content with quantities independent of absolute entropy, such as pressure. As a result, the lack of knowledge of the absolute entropy on the high-density equation of state branch for rigid disks, coupled with the relatively large virial fluctuations in the transition region, has so far prevented accurate location of the (apparently first-order) transition, both in pressure and in coexistent phase densities.

The major purpose of the present paper is the evaluation of the absolute free energy of the rigid-disk system at very high compressions. We find that the Helmholtz free energy per particle (divided by kT), has an asymptotic expansion of the form

$$F/NkT \sim 2\ln(\lambda/a) - 2\ln(\theta^{-1}-1) + C + D(\theta^{-1}-1) + \cdots. \quad (1)$$

(λ is the mean thermal de Broglie wavelength) in which the leading logarithmic term involving θ is the one predicted by a single particle ("free area") approximation, and the additive free energy constant C may be expressed as an infinite series. In Eq. (1),

* Summer visitor at Murray Hill, 1964; permanent address: Chemistry Department, Rice University, Houston, Texas.

[1] B. J. Alder and T. E. Wainwright, Phys. Rev. 127, 359 (1962); W. W. Wood, "Monte Carlo Calculations of the Equation of State of Systems of 12 and 48 Hard Circles" (Los Alamos Scientific Laboratory, Los Alamos, New Mexico, 1963), Report LA-2827.

θ is the reduced density whose maximum value, unity, is attained at close packing.

The first few terms of the C series are evaluated here, and as shown in Sec. V, the result may be used in conjunction with Monte Carlo or molecular-dynamic pressures for the rigid-disk system to obtain first the absolute Helmholtz free energy vs system area for *both* phases. A Maxwell double-tangent construction[2] thereupon locates precisely the transition pressure and densities. In this manner one circumvents in principle the ambiguity produced by pressure fluctuations or metastability in the transition region of density.

The limiting free-energy expression (1) may be considered a high density analog of the imperfect gas virial expansion, a power series in θ. But unlike the low-density virial series for F/NkT which is known to possess a finite radius of convergence,[3] Eq. (1) is only an asymptotic series. Ironically, it is the high-compression analogs of the low-density fluid particles, the vacancies in the crystal, which prevent convergence to the correct free energy, for as is shown in Sec. III, their contribution to F/NkT exhibits an essential singularity at $\theta=1$. It is worth stressing at this point that the present situation is in distinct contrast to any lattice-gas approximation to the rigid-disk system, since for these latter the vacancies play a central role at high density, and hence yield a different type of dominant free-energy singularity as θ approaches unity.[4]

Our theoretical program is initiated in the next section. Disk configurations are classified by means of a reference lattice of points chosen to be a regular hexagonal lattice, consistent with the close-packed crystal structure. An identity is then displayed for the exact rigid-disk partition function Q_N, consisting of factors referring to cooperative motion of connected subsets of the disks. Section III shows why vacancies in the actual disk arrangements may be disregarded for the purposes of calculating high-density limiting behavior.

The specific problem of evaluating the additive free-energy constant C is analyzed in Sec. IV. An infinite series for C is deduced whose terms are in one-to-one correspondence with a subset of all connected graphs that may be drawn on the planar hexagonal lattice. Each such term requires evaluation of the content of a multidimensional polytope. Terms of the C series corresponding to graphs of four or fewer vertices are numerically evaluated. The result analyzed in Sec. V indicates that a single-particle "free-area" estimate of C (actually the first term of the C series), gives slightly too high an additive free-energy constant. Section IV points out that our C series is similar but not identical to the one that can be obtained from the de Boer cell-cluster theory.

By way of justifying treatment of the infinite C series (ordering the terms according to ascending numbers of vertices in the associated graphs), the case of rigid rods in one dimension is worked out exactly in an Appendix. The corresponding infinite series for the one-dimensional additive free-energy constant converges to the correct value.

The type of approach exploited here is not restricted to rigid disks but may, with certain obvious elaborations, be applied to three-dimensional rigid spheres. Although we reserve detailed computations on this latter model for a subsequent publication, a few comments on rigid-sphere crystal stability appear in the discussion of Sec. VI.

The calculation of rigid-particle additive free-energy constants is equivalent to finding the hypervolume of the limiting polytope accessible to the many-particle system in the full configuration space.[5] By way of illustrating the fundamental difficulty that multidimensional geometry poses to statistical mechanics, we remark in passing that the obvious strategy of inscribing and circumscribing hyperspheres in and about this polytope to deduce rigorous bounds on C, succeeds only in establishing that this quantity lies between plus and minus infinity! We offer the analysis below as a more successful approach.

II. GENERAL THEORY

We examine a set of N identical rigid (nonoverlapping) disks of diameter a whose centers are confined to an area A in the plane. Although the disks eventually are assumed to be nearly close packed over A, our general considerations in this section are valid, in principle, independent of the system density.

Let A be covered by a regular hexagonal array of M points, where the integer M is limited to values

$$N \leq M \leq N_{\max}; \tag{2}$$

$N_{\max}$ stands for the maximum number of disks which may be placed with centers in A in a regular hexagonal array.[6] Furthermore, let $\mathbf{s}_1 \cdots \mathbf{s}_M$ denote the positions of these M "reference points".

In order to calculate the various thermodynamic properties of the system, it is necessary to evaluate the rigid-disk partition function

$$Q_N = (\lambda^{2N} N!)^{-1} \int \cdots \int \prod_{i<j=1}^{N} \phi(ij)\, d\mathbf{r}_1 \cdots d\mathbf{r}_N; \tag{3}$$

$$\varphi(ij) = 0 \qquad (r_{ij} \leq a)$$

$$= 1 \qquad (r_{ij} > a).$$

[2] J. S. Rowlinson, *Liquids and Liquid Mixtures* (Butterworths Scientific Publications, Ltd., London, 1959), p. 80.

[3] J. Groeneveld, Phys. Letters **3**, 50 (1962); E. Lieb, J. Math. Phys. **4**, 671 (1963); O. Penrose, *ibid.*, pp. 1312, 1488; J. L. Lebowitz and J. K. Percus, *ibid.*, p. 1495.

[4] F. H. Stillinger, Jr., E. A. Di Marzio, and R. L. Kornegay, J. Chem. Phys. **40**, 1564 (1964); W. G. Hoover, B. J. Alder, and F. H. Ree, *ibid.* **41**, 3528 (1964).

[5] Z. W. Salsburg and W. W. Wood, J. Chem. Phys. **37**, 798 (1962).

[6] It is the intent of this paper to focus attention solely on bulk thermodynamic properties of the rigid-disk system. For this reason we consistently disregard the special character of disks in the boundary region.

The configuration integrals in Eq. (3) span the area A. We use the set of reference points to aid in calculating Q_N. P now stands for an ordered subset of N of the M sites, and in particular $\mathbf{s}_{Pi}$ is the site position of the ith member of this ordered subset.

For any given set of particle center positions, and a particular site-subset choice P, one may compute the quantity

$$R_P^2=\sum_{i=1}^{N}(\mathbf{r}_i-\mathbf{s}_{Pi})^2. \tag{4}$$

Aside from an unimportant class of disk configurations of zero measure, there will exist an unique ordered subset P of reference sites which minimizes the quantity R_P. Also for a given P, the set of configurations $\mathbf{r}_1\cdots\mathbf{r}_N$ for which R_P is a minimum is some connected, convex region $\Omega(P)$ in the entire $2N$-dimensional configuration space for the disks. The partition function Q_N may therefore be written in the following form:

$$Q_N=(\lambda^{2N}N!)^{-1}\sum_P\int_{\Omega(P)}\cdots\int\prod_{i<j=1}^{N}\phi(ij)d\mathbf{r}_1\cdots d\mathbf{r}_N, \tag{5}$$

where in each member of the P sum, integration is restricted only to region $\Omega(P)$. Since there are always precisely $N!$ subsets P which differ only in the ordering of chosen sites, and since each of these gives an identical contribution to Q_N, Eq. (5) simplifies to

$$Q_N=\lambda^{-2N}\sum_P{}'\int_{\Omega(P)}\cdots\int\prod_{i<j=1}^{N}\phi(ij)d\mathbf{r}_1\cdots d\mathbf{r}_N, \tag{6}$$

where now the primed P summation includes only distinct subsets of sites irrespective of ordering. From now on we may suppose that for a given P the particles and sites have been so named that $\Omega(P)$ is defined in Eq. (4) by pairing Particle 1 with Site $\mathbf{s}_1$, $\cdots$, Particle N with Site $\mathbf{s}_N$.

We are now in a position to write down an identity for Q_N. To do so, a set of correlated disk-motion configuration integrals are defined. The first refers to a single movable disk (i) in a field of $N-1$ disks confined to the reference sites

$$Z_i(P)=\int_{\omega_i(P)}\prod_{\substack{j=1\\(\neq i)}}^{N}\phi(ij)d\mathbf{r}_i,$$

$$\mathbf{r}_j=\mathbf{s}_j\qquad(j\neq i). \tag{7}$$

$\omega_i(P)$ is that region in the two-dimensional configuration space of Particle i such that the set of configurations for i and the remaining $N-1$ constrained disks lies in $\Omega(P)$. In a similar fashion, $Z_{ij}(P)$, $Z_{ijk}(P)$, etc., stand for configuration integrals for a pair (ij), a triplet (ijk), etc., of movable particles in a field consisting of the residual set of disks at the fixed set of reference sites dictated by P:

$$Z_{ij}(P)=\iint_{\omega_{ij}(P)}\phi(ij)\Big[\prod_{\substack{k=1\\(\neq i,j)}}^{N}\phi(ik)\phi(jk)\Big]d\mathbf{r}_id\mathbf{r}_j,$$

$$Z_{ijk}(P)=\iiint_{\omega_{ijk}(P)}\phi(ij)\phi(ik)\phi(jk)\times\Big[\prod_{\substack{l=1\\(\neq i,j,k)}}^{N}\phi(il)\phi(jl)\phi(kl)\Big]d\mathbf{r}_id\mathbf{r}_jd\mathbf{r}_k,\quad\text{etc.} \tag{8}$$

The regions $\omega_{ij}(P)$, $\omega_{ijk}(P)$, etc. are defined by the requirement that the full set of free-plus-fixed-particle center positions lies within the $2N$-dimensional region $\Omega(P)$.

The desired Q_N is expressed as a formally exact product of factors for each P, the leading set of which corresponds to contributions of single particles, then a set which corrects for correlated motion of disk pairs, then triplet correlation corrections, and so on:

$$\begin{aligned}Q_N&=\lambda^{-2N}\sum_P{}'\Big\{\prod_{i=1}^{N}Z_i(P)\Big\}\Big\{\prod_{i<j=1}^{N}\frac{Z_{ij}(P)}{Z_i(P)Z_j(P)}\Big\}\\&\quad\times\Big\{\prod_{i<j<k=1}^{N}\frac{Z_{ijk}(P)Z_i(P)Z_j(P)Z_k(P)}{Z_{ij}(P)Z_{ik}(P)Z_{jk}(P)}\Big\}\cdots\\&=\lambda^{-2N}\sum_P{}'\Big\{\prod_{i=1}^{N}Y_i(P)\Big\}\Big\{\prod_{i<j=1}^{N}Y_{ij}(P)\Big\}\\&\quad\times\Big\{\prod_{i<j<k=1}^{N}Y_{ijk}(P)\Big\}\cdots\{Y_{1\cdots N}(P)\}.\end{aligned} \tag{9}$$

The last factor in this product representation of the contributions to Q_N, $Y_{1\cdots N}(P)$, will contain a single $Z_{1\cdots N}(P)$ in its numerator, and lower order Z's in both numerator and denominator. With inclusion of this last factor, Eq. (9) becomes an identity, with Z's of lower than Nth order cancelling between numerators and denominators, to leave precisely Eq. (6). By definition the correction factor $Y_{1\cdots n}(P)$ for an arbitrary set of n particles may be obtained simply by writing:

$$Y_{1\cdots n}(P)=Z_{1\cdots n}(P)/\prod_{\text{subsets}}Y_{\alpha\cdots\nu}(P), \tag{10}$$

where the denominator contains a product of Y's, one factor for each proper subset of disks $1\cdots n$.

III. ROLE OF VACANCIES

Although Eq. (9) retains its formal exactness at low densities, one recognizes that the utility of such a product representation of Q_N depends upon rapid convergence to unity of the individual factors, and intuitively one would expect such convergence only if the "reference state" (particles confined to the

hexagonal lattice) is a reasonable description of the physical state. We now restrict attention to the highly compressed "crystalline" state for disks.

It is our main objective to examine the limiting behavior of the Helmholtz free energy per particle (divided by kT):

$$F/NkT=-N^{-1}\ln Q_N \tag{11}$$

as the density of particles approaches its absolute geometric upper limit

$$N_{\max}/A=2/\sqrt{3}a^2. \tag{12}$$

In order to illustrate the method of using the product representation (9), as well as to establish the relative importance of defects in the regular disk arrangements for limiting free energy, we temporarily truncate each term in the P sum of Eq. (9) after the single-particle factors. This serves to determine the asymptotic behavior of F/NkT. We finally see at the end of this section that reinsertion of pair, triplet, etc. factors does not affect the general conclusions.

It is convenient to use a dimensionless density variable:

$$\theta=\sqrt{3}Na^2/2A, \tag{13}$$

whose value at close packing is unity. When θ is slightly less than unity the state of packing of the disks will not be perfect, but defects can be expected to occur. Figure 1 shows a portion of a configuration of disks, placed at reference sites from which they wander, including both monovacancies and divacancies. As shown, the integrand regions for the various factors $Y_i=Z_i$ differ according to the number of neighboring disks.

An elementary calculation allows one to find Z_i for a disk with six fixed neighboring disks[7]:

$$Z_i=\left\{\frac{3\sqrt{3}}{2\theta_0}-\frac{3}{\theta_0^{\frac{1}{2}}}\left(1-\frac{1}{4\theta_0}\right)^{\frac{1}{2}}-2\pi+6\cos^{-1}\frac{1}{2\theta_0^{\frac{1}{2}}}\right\}a^2, \tag{14}$$

$$\theta_0=M\theta/N. \tag{15}$$

This expression is the area of the regular "hexagon," bounded by circular arcs, over which a particle may freely wander when confined by the six fixed neighbors. As θ_0 approaches unity, this area becomes smaller and its boundary curvature becomes negligible to yield in the limit a regular hexagon with area:

$$Z_i\sim(\tfrac{1}{2}\sqrt{3}a^2)\,(\theta_0^{-1}-1)^2. \tag{16}$$

The six disks neighboring a monovacancy each have an area larger than the result (14), as Fig. 1 shows. In the $\theta_0\to1$ limit, it is easy to see that the previous hexagon has now an extra equilateral triangle on the side toward the vacancy, giving a result $\frac{7}{6}$ as large as (16):

$$Z_i\sim(\tfrac{7}{6})\,(\tfrac{1}{2}\sqrt{3}a^2)\,(\theta_0^{-1}-1)^2. \tag{17}$$

In the case of divacancies (we do not consider more complicated defects), there are two types of neighboring disks. Six of them have five neighbors, and therefore lead to the same Z_i limiting value (17) as for monovacancy-neighboring disks. The remaining two, however, possess an area which does *not* vanish as $\theta_0\to1$, but instead approaches:

$$Z_i\sim[(\tfrac{1}{3}\sqrt{3})-(\tfrac{1}{6}\pi)]a^2. \tag{18}$$

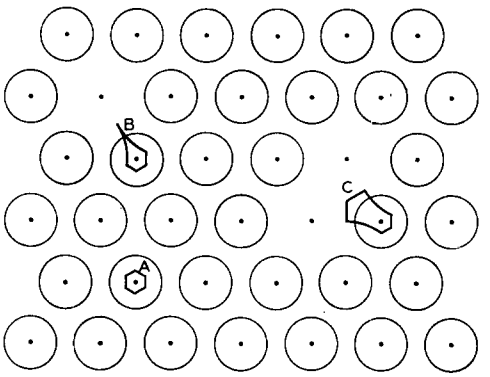

FIG. 1. An arrangement of disks on the reference sites, showing a monovacancy and a divacancy. The figures A, B, and C are, respectively, the allowed regions of integration for the Z_i in the cases of six, five, and four nearest-neighbor disks to the disk (i) under consideration.

It is a general property of the complete Q_N expression, Eq. (9), that it should yield a result independent of the choice of M within the allowed range (2). A truncated approximation, though, will not exhibit this property. In particular, variations with M of the single particle factors Z_i should in principle be canceled by M variations of succeeding pair, triplet, etc. terms, but for our present illustrative calculation this cannot be included. In order to obtain the best single-particle description, we employ this M variation to minimize the free energy, and thus obtain an estimate of the manner in which the number of vacancies in the disk arrangement varies as the assembly is compressed to its geometric limit.

In the high-compression limit, both monovacancies and divacancies are rare. Letting N_d denote the number of divacancies in the arrangement, the number N_m of monovacancies will be

$$N_m=M-N-2N_d. \tag{19}$$

On account of vacancy rarity, we may use a random-mixing approximation to represent adequately the number of distinct ways $W(M, N, N_d)$ to distribute the $M-N_d$ entities (N disks, N_m monovacancies, and N_d divacancies) over the lattice of reference sites[8]

$$W(M,N,N_d)\cong\left[\frac{M!}{N_d!(M-N_d)!}\right]3^{N_d}\left[\frac{(M-2N_d)!}{N_m!N!}\right]$$

$$=\frac{3^{N_d}M!(M-2N_d)!}{N!N_d!(M-N_d)!(M-N-2N_d)!}. \tag{20}$$

[7] This result requires $\frac{1}{2}\leq M\theta/N\leq1$.

[8] The three contributing factors are (1) number of ways of selecting a site for one end of divacancies, (2) three orientations for each divacancy, (3) number of ways of placing disks and monovacancies over remaining $M-2N_d$ sites.

In our present single-particle factor approximation, we therefore have

$$Q_N(M)=\lambda^{-2N}\sum_{N_d=0}^{\frac{1}{2}(M-N)} W(M,N,N_d)$$
$$\times\left[\tfrac{1}{2}\sqrt{3}a^2(\theta_0^{-1}-1)^2\right]^{N-2N_d}\left[\tfrac{7}{6}\right]^{6N_m+6N_d}\left[(\tfrac{1}{3}\sqrt{3}-\tfrac{1}{6}\pi)a^2\right]^{2N_d}, \quad (21)$$

where results (16), (17), and (18) have been inserted.

In the usual manner, the bulk-phase free energy per particle may be obtained from the maximum term of the summand in Eq. (21). Its value, as well as the equilibrium values of M and N_d will be found from the two extremum conditions on the logarithm of the summand. Treating these as continuous variables, and using Stirling's factorial formula, one finds that the system free energy has the form

$$-F_N(M,N_d)/kT=-2N\ln\lambda+N_d\ln 3+M\ln M$$
$$+(M-2N_d)\ln(M-2N_d)-N\ln N$$
$$-N_d\ln N_d-(M-N_d)\ln(M-N_d)$$
$$-(M-N-2N_d)\ln(M-N-2N_d)$$
$$+(N-2N_d)\ln\{\tfrac{1}{2}\sqrt{3}a^2[(N/M\theta)-1]^2\}$$
$$+6(M-N-N_d)\ln(\tfrac{7}{6})+2N_d\ln[(\tfrac{1}{3}\sqrt{3}-\tfrac{1}{6}\pi)a^2]. \quad (22)$$

Next differentiate with respect to M and to N_d, and set the results equal to zero, to obtain the equations,

$$\frac{(M-N-2N_d)(M-N_d)}{M(M-2N_d)}=(\tfrac{7}{6})^6\exp\left[-\frac{2N(N-2N_d)}{M^2\theta[(N/M\theta)-1]}\right], \quad (23)$$

$$\frac{N_d(M-2N_d)^2}{(M-N-2N_d)^2(M-N_d)}=\frac{4(\frac{8}{7})^6(\frac{1}{3}\sqrt{3}-\frac{1}{6}\pi)^2}{[(N/M\theta)-1]^4}. \quad (24)$$

This pair of coupled nonlinear equations, for a given value of θ, determines the value of M and N_d which extremalize the single-particle approximation to the free energy.

It is apparently not possible to find the general solutions to Eqs. (23) and (24) in closed form, but as $\theta\to 1$, the limiting behaviors may readily be extracted. One knows physically that as θ approaches unity, N_d will become very small, and N approaches M, i.e., the disk packing becomes more perfect. Consequently, Eqs. (23) and (24) approach the $\theta\cong 1$ forms

$$\frac{N_m}{M}=(\tfrac{7}{6})^6\exp\left[-\frac{2}{\theta^{-1}-1}\right], \quad (25)$$

$$\frac{(N_d/M)}{(N_m/M)^2}=4(\tfrac{8}{7})^6(\tfrac{1}{3}\sqrt{3}-\tfrac{1}{6}\pi)^2(\theta^{-1}-1)^{-4}. \quad (26)$$

These last two equations give, respectively, the equilibrium concentration of monovacancies at high compression, and the corresponding "chemical equilibrium constant" for association of two monovacancies to form a divacancy.

Equation (25) is a key result, for it states that the concentration of monovacancies is proportional to the essentially singular function $\exp[-2/(\theta^{-1}-1)]$. Therefore as θ approaches unity, N_m/M vanishes faster than any positive power of $(\theta^{-1}-1)$. In spite of the fact that divacancies afford considerable movement freedom for a few neighboring disks [this favorable divacancy feature at high compression leads to the divergent factor $(\theta^{-1}-1)^{-4}$ on the right side of Eq. (26)], their concentration N_d/M vanishes even more strongly since two such essentially singular factors are involved.[9] Returning to the free-energy expression (22), one can now see that the contribution of vacancies to F likewise will vanish faster than any positive power of $(\theta^{-1}-1)$.

On account of this strong vanishing of vacancy contributions, it is justifiable to assume asymptotically at high compression that the arrangement of disks is perfect ($M=N$). In the single-particle approximation, therefore, the free energy is predicted to be

$$F/NkT\cong 2\ln\lambda-\ln Z_i(\theta), \quad (27)$$

where $Z_i(\theta)$ is the single-particle integral for six neighbors, given in Eq. (14) (remembering now $\theta_0=\theta$). Near $\theta=1$, Eq. (27) will admit of an expansion of the following type:

$$F/NkT\sim 2\ln(\lambda/a)-2\ln(\theta^{-1}-1)+C_1$$
$$+D_1(\theta^{-1}-1)+E_1(\theta^{-1}-1)^2+\cdots. \quad (28)$$

The leading logarithmic terms are known to be rigorously correct for finite systems,[5] and succeeding terms beyond C_1 arise in part from deviation of integration regions [the ω's in Eqs. (7) and (8)] from straight-sided polygons. The value of C_1 is found to be

$$C_1=-\ln\tfrac{1}{2}\sqrt{3}=0.14384. \quad (29)$$

An expansion of the form (28) cannot converge to the correct free energy, since we have seen that there is at least one class of contributions due to vacancies which cannot be so expanded. Therefore an expansion of Type (28), with suitable numerical coefficients C, D, E, $\cdots$ can at best be an *asymptotic* expansion.

In the next section we consider revision of the single-particle truncation by inclusion of sets of Y's in Eq. (9) for larger numbers of particles. First, however, one must be assured that such corrections do not overturn the principal result just found concerning the noncontribution of vacancies. In the $\theta\to 1$ limit, we shall see that each Y for two or more disks approaches a constant of order unity.[10] These extra factors would show up in a more accurate version of the variational free-energy expression (22) as terms linear in M and N_d.

[9] It is clear that larger vacancies, if they had been included in the calculation, would have had more such unfavorable factors in their equilibrium concentration expressions.

[10] Although Sec. IV considers only the perfect disk crystal, the same result is true for Y's in the defective crystal case.

Simultaneous Eqs. (23) and (24) would therefore have one member multiplied by constants of order unity, but this would not affect the conclusion concerning the essentially singular nature of vacancy concentrations or their free-energy contributions. We may therefore proceed to calculate the additive free-energy constant C in the correct asymptotic series (1) from perfect crystal Y's.

IV. ADDITIVE FREE-ENERGY CONSTANT

The high-compression form of Eq. (9) which we use to calculate C is the single product:

$$Q_N(\theta)=\lambda^{-2N}\{\prod_{i=1}^{N}Y_i(\theta)\}\{\prod_{i<j=1}^{N}Y_{ij}(\theta)\}$$
$$\times\{\prod_{i<j<k=1}^{N}Y_{ijk}(\theta)\}\cdots\{Y_{1\cdots N}(\theta)\} \quad (30)$$

for the perfect crystal. It is easy to see that many of the Y's formally included here will actually be unity and may be disregarded. The factors $Y_{ij}=Z_{ij}/Z_iZ_j$, for example, in the case that Disks i and j are not nearest neighbors, consists of a numerator Z_{ij} which necessarily factors into $(Z_i)(Z_j)$, the denominator, since the two particles cannot interact. It is similarly possible to show by induction from Eq. (10) that the only nonunity Y's are those whose subscripted particles form a connected set, i.e., any disk may be reached from any other by jumping to nearest neighbors within the set only.

Even among the remaining nontrivial factors in Eq. (30), many involving the same number of disks will give identical factors. In particular, all nearest-neighbor pairs will yield the same Y_{ij}, reflecting an orientation and translation invariance in the lattice of disks. We henceforth denote this contribution simply by $Y^{(2,1)}(\theta)$ and note that it occurs once for each nearest-neighbor pair in the disk crystal, that is, $3N$ times.

There are three types of connected disk triplets: a linear triplet, an obtuse triplet (central angle 120°), and a compact equilateral triangle. We denote the corresponding factors in Eq. (30) by $Y^{(3,1)}(\theta)$, $Y^{(3,2)}(\theta)$, and $Y^{(3,3)}(\theta)$, respectively. Table I catalogs the independent types of connected subsets involving five or fewer disks along with the "lattice factor" $l(n, \alpha)$ equal to N^{-1} times the number of distinct such subsets in the N-disk crystal.[11] The number of different connected topological subset types for a given number n of disks obviously increases very rapidly with n.

Evaluation of the additive free-energy constant C requires θ to approach unity in Eq. (30), and each factor (besides those for single particles) approaches in this limit some nonzero constant for which we simply write $Y^{(n,\alpha)}$ (the last column in Table I). In view of Eqs. (1), (28), (29), and (30), we find that the additive free-energy constant has the expansion:

$$C=-\ln\tfrac{1}{2}\sqrt{3}-\sum_n[\sum_\alpha l(n,\alpha)\ \ln Y^{(n,\alpha)}]. \quad (31)$$

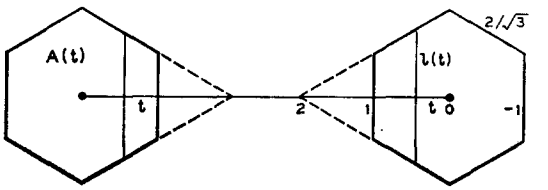

FIG. 2. Regions available for motion of two neighboring correlated disks, in the high compression limit (straight boundaries). The unit of length has been chosen so that the side of the regular single-disk free-area hexagon is $2\sqrt{3}$. If the particle on the right has been displaced to the left by distance t (as projected along the center line) the corresponding boundary of the other particle's cell is displaced by the same amount to leave, generally, area $A(t)$. The allowed values of t are $-1\leq t\leq 2$. Since this refers to the high compression limit the cell size relative to the site–site distance has been greatly exaggerated.

The terms in Eq. (31) for C have been ordered by number of correlated particles, n. Although we know of no rigorous way of demonstrating convergence for (31), the Appendix shows that for the analogous case of rigid rods in one dimension the series does indeed converge to the correct result. The evaluation of the first few terms in (31) as we see is also consistent with convergence in two dimensions, and so we tentatively propose to accept as valid the ordering of terms shown in Eq. (31).

A. Correlated Pair Integral

We proceed to calculate the leading contributions to the infinite sum in Eq. (31) for the rigid-disk system. The first, and simplest, contribution encountered is

$$Y^{(2,1)}=\lim_{\theta\to 1}Z^{(2,1)}(\theta)/[\tfrac{1}{2}\sqrt{3}a^2(\theta^{-1}-1)^2]^2. \quad (32)$$

Figure 2 shows the regions of motion of the two neighboring particles correlated by $Z^{(2,1)}(\theta)$, for sufficiently small θ that straight boundaries apply. Since (32) consists of a dimensionless ratio of integrals, we may choose any convenient length unity; in particular the side of the regular hexagonal free area for single particles with six fixed neighbors is taken to be $2/\sqrt{3}$.

Reference to Fig. 2 demonstrates that the effect of allowing simultaneous motion of a neighboring pair is that as one disk moves from its reference site, the boundary for motion of the other disk which it provides by virtue of the repulsive interaction also moves an equal distance. If t denotes the projection of one disk's motion from its reference site along the line to the neighbor-disk's reference site, then Fig. 2 shows that the pair correlation factor $Y^{(2,1)}$ may be written as

$$Y^{(2,1)}=[A(0)]^{-2}\int_{-1}^{2}l(t)\,A(t)\,dt, \quad (33)$$

where $l(t)$ is the length of travel permitted a particle (direction perpendicular to the site–site direction) by

[11] Mirror-image subsets are not distinguished.

TABLE I. Catalog of the various species of connected sets of disks including five or fewer particles. The solid bonds in the graphs indicate nearest neighbors. Y's reported in the text are included.

Cluster graph	Cluster number n, α	$t(n, \alpha)$	$Y^{(n,\alpha)}$
	2, 1	3	$\frac{217}{216}$
	3, 1	3	$\frac{233\ 208}{235\ 445}$
	3, 2	6	$\frac{235\ 488}{235\ 445}$
	3, 3	2	$\frac{51\ 430\ 464}{51\ 091\ 565}$
	4, 1	3	$\frac{501\ 875\ 275}{503\ 573\ 808}$
	4, 2	12	$\frac{253\ 890\ 775}{254\ 248\ 544}$
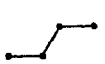	4, 3	6	$\frac{1\ 539\ 756\ 825}{1\ 540\ 405\ 504}$
	4, 4	6	
	4, 5	2	$\frac{121\ 215\ 650\ 311\ 875}{120\ 915\ 670\ 441\ 984}$
	4, 6	12	$\frac{985\ 154\ 855\ 125}{984\ 351\ 143\ 424}$
	4, 7	3	1.005941
	5, 1	3	
	5, 2	12	
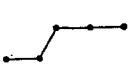	5, 3	12	
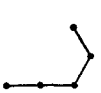	5, 4	12	
	5, 5	6	
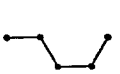	5, 6	12	

Cluster graph	Cluster number n, α	$t(n, \alpha)$	$Y^{(n,\alpha)}$
	5, 7	6	
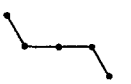	5, 8	6	
	5, 9	6	
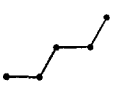	5, 10	6	
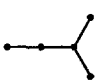	5, 11	6	
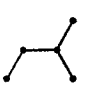	5, 12	12	
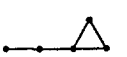	5, 13	12	
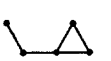	5, 14	12	
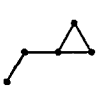	5, 15	12	
	5, 16	6	
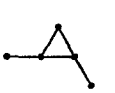	5, 17	12	
	5, 18	6	
	5, 19	3	
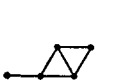	5, 20	12	
	5, 21	6	
	5, 22	6	

the remaining fixed boundaries, and $A(t)$ is the hexagonal area with one boundary displaced by t.

In the units chosen, one easily finds

$$l(t)=(2/\sqrt{3})(2+t) \qquad -2\leq t\leq 0$$
$$=(2/\sqrt{3})(2-t) \qquad 0\leq t\leq 2. \tag{34}$$

Also, since

$$A(t)=\int_{-1}^{1-t} l(t')\,dt', \tag{35}$$

we have:

$$A(t)=(2/\sqrt{3})(3-t-\tfrac{1}{2}t^2) \qquad -1\leq t\leq 1$$
$$=(2/\sqrt{3})(4-3t+\tfrac{1}{2}t^2) \qquad 1\leq t\leq 2. \tag{36}$$

Insertion of the explicit forms (34) and (36) into (33) leads to the pair correlation result:

$$Y^{(2,1)}=\frac{217}{216}, \tag{37}$$

which is recorded in the last column of Table I.

B. Triplet Integrals

The linear triplet, designated (3, 1) in Table I, is conceptually no more complicated than the pair case, if attention is focused on the central disk position. As before, Fig. 3(a) shows its displacement projected on the horizontal to be denoted by t, and the areas available to the end disks then are $A(t)$ and $A(-t)$. Taking proper account of the denominator factors in Eq. (10), one has:

$$Y^{(3,1)}=\{[A(0)]^3[Y^{(2,1)}]^2\}^{-1}2\int_0^2 l(t)\,A(t)\,A(-t)\,dt, \tag{38}$$

where now Eqs. (36) must be supplemented by the fact that $A(t)$ is the constant $A(-1)$ for $-2\leq t\leq -1$.

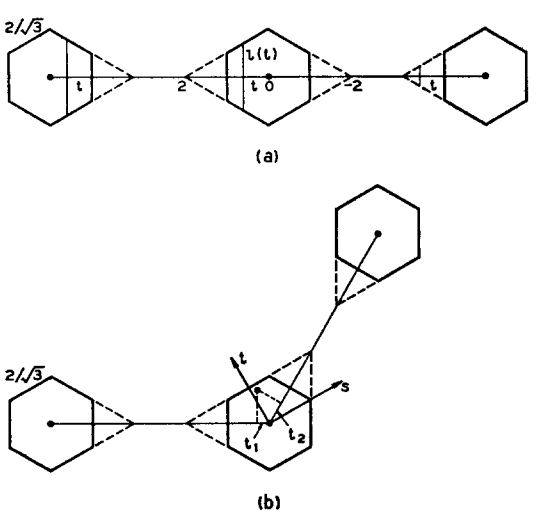

FIG. 3. Coordinate systems used for evaluating (a) $Y^{(3,1)}$ and (b) $Y^{(3,2)}$. For the latter, t_1 and t_2 are projected distances along the two site–site center lines of the displacement of the central particle.

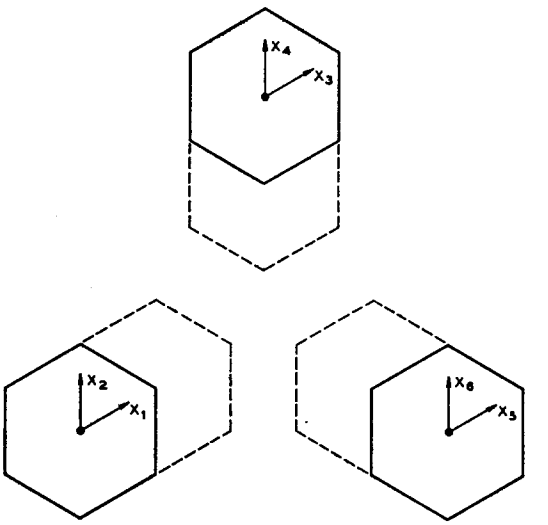

FIG. 4. Boundaries and oblique coordinates used in evaluation of $Y^{(3,3)}$ by ALPAK.

Although the central disk displacement may be anywhere between -2 and 2, the symmetry of the triplet insures that twice the integral over positive t suffices, as written in (38). Carrying out the indicated operations, one finds

$$Y^{(3,1)}=\frac{233\,208}{235\,445}. \tag{39}$$

The case (3, 2) is somewhat complicated by the fact of noncollinearity. One sees in Fig. 3(b) that a rectangular coordinate system (s, t) has been placed on the central site, with one axis (t) bisecting the obtuse graph angle. The two projections, t_1 and t_2, along the site–site directions are then found to be:

$$t_1=\tfrac{1}{2}t+\tfrac{1}{2}\sqrt{3}s,$$
$$t_2=\tfrac{1}{2}t-\tfrac{1}{2}\sqrt{3}s. \tag{40}$$

In the same fashion as previously, one writes

$$Y^{(3,2)}=\{[A(0)]^3[Y^{(2,1)}]^2\}^{-1}$$
$$\cdot 2\int_{-1}^{1}dt\int_0^{(3)^{-1}(2+t)} ds\,A[t_1(s,t)]A[t_2(s,t)]. \tag{41}$$

Due largely to the fact that the functional form of the A's changes across oblique boundaries in the (s, t) space, the work required in evaluation of (41) is relatively lengthy; the result is

$$Y^{(3,2)}=\frac{235\,488}{235\,445}. \tag{42}$$

Figure 4 shows that in the (3, 3) case, the outer extremes of motion for any of the three disk centers in this compact cluster, form an elongated hexagon. Although computation of any $Y^{(n,\alpha)}$ involves only sets of iterated integrals of polynomials between linear binomial limits, the three movable boundaries in this

last triplet type cause the necessary algebra to be extremely tedious, and thereby greatly susceptible to human error. Accordingly, $Y^{(3,3)}$ was first obtained by a Monte Carlo estimate with the approximate result,

$$Y^{(3,3)} \cong 1.0088 \pm 0.0021, \tag{43}$$

where the quoted errors represent 95% confidence limits assigned on the basis of a Gaussian fit to the expected result distribution.

Since the $Y^{(n,\alpha)}$ tend to be very close to unity, and since they enter the C series in logarithmic form, Monte Carlo errors such as shown in (43) become amplified in relative importance. Because of this fact, and also because $Y^{(3,3)}$ is required by Eq. (10) in construction of higher order $Y^{(n,\alpha)}$'s, it was decided to use the ALPAK system on the Murray Hill IBM 7094 computer to perform the integrations directly and exactly. In order to facilitate computer use, the basic $Y^{(3,3)}$ integral was set up using oblique coordinates with axes parallel to cell sides as shown in Fig. 4. Although we do not present details here the multiple integrals with these oblique coordinates may be taken between constant integer limits, and the integrand becomes a product of unit step functions whose arguments are linear combinations of the oblique coordinates with coefficients ± 1. In this manner, it was found that

$$Y^{(3,3)} = \frac{51\,430\,464}{51\,091\,565}. \tag{44}$$

Besides confirming and sharpening the Monte Carlo estimate (43), the ALPAK program also verified the previously quoted $Y^{(2,1)}$, $Y^{(3,1)}$, and $Y^{(3,2)}$ results when these other integrals were cast into the required canonical oblique coordinate system form.

C. Quadruplet Integrals

Table I lists the seven distinct four-particle integrals that must be evaluated for the C series. Of these seven, $Y^{(4,1)}$ and $Y^{(4,5)}$ are, relatively speaking, the simplest to perform manually, and consequently were evaluated at considerable time expense to provide extra checks on the ALPAK program. These two results, as well as the other five which could be performed only by computer using the standard oblique coordinate representation are assembled in Table I. In case (4, 7), computer limitations permitted only the decimal equivalent to be obtained.

D. Results

The final numerical values of the successive terms in the C series (for $n=1, 2, 3, 4$) are found from Table I to be

$$C = 0.14384 - 0.01386 + 0.014322 - 0.00061 + \cdots. \tag{45}$$

Here the α summation for given n has already been performed. Assuming that the total contribution of all terms beyond those shown explicitly in Eq. (45) is negligible,

$$C \cong 0.14370, \tag{46}$$

representing a slight decrease below the "free-area" approximation. It is interesting to compare the two-dimensional C series (45) with its one-dimensional analog for rigid rods, worked out completely in the Appendix. Compared with this latter example, the terms following the first in Eq. (45) are relatively smaller corrections, and indeed are the result of partially cancelling contributions. On the basis of the calculation as far as we have carried it, therefore, it tentatively appears that "collective motions" play a relatively smaller part in determining the absolute entropy of rigid disks near close packing, compared to rigid rods.

V. ANALYSIS OF MACHINE CALCULATIONS

The basis for use of the computed additive free-energy constant C is the famous Maxwell double tangent construction,[2] which is to be carried out on Helmholtz free-energy curves vs θ^{-1}. We assume that the "input data" from machine-computed rigid-disk equations of state are available for both high- and low-density phases in the form of the compressibility factor

$$K(\theta) = pA/NkT. \tag{47}$$

In the low-density region, the elementary thermodynamic relation

$$p = -(\partial F/\partial A)_{N,T}, \tag{48}$$

along with knowledge of the ideal gas free-energy appropriate to zero density, allows (47) to be integrated to yield the fluid phase (Subscript f) Helmholtz free-energy per disk:

$$\frac{F_f(\theta^{-1})}{NkT} = \ln\frac{2\theta}{\sqrt{3}e} + \int_0^\theta [K_f(\theta') - 1]\frac{d\theta'}{\theta'}. \tag{49}$$

For the "solid" phase (Subscript s), we may obtain the analogous free energy expression by integrating between the θ value of interest and unity, rather than zero. The requisite integration constant, as well as a convergence-producing integrand subtraction, are provided by the asymptotic expression (1). One finds:

$$\frac{F_s(\theta^{-1})}{NkT} = -2\ln(\theta^{-1}-1) + C - \int_\theta^1 \left[K_s(\theta') - \frac{2}{1-\theta'}\right]\frac{d\theta'}{\theta'}. \tag{50}$$

Unlike the high-compression asymptotic series, the integral term in (50) properly provides even the essentially singular vacancy, etc., contributions.

The characteristic metastability that may be achieved on both fluid and solid isotherm branches in finite-system machine computations, implies that both Eqs. (49) and (50) may in practice be numerically integrated well past the double tangency points.

Although the currently available machine pressures do not permit very precise integrations of (49) and (50), we have been able to verify that they are roughly consistent with the postulated transition. It is our hope that the results obtained in this paper will stimulate calculation of accurate fluid and solid pressures for closely spaced values of θ over the entire density range, to allow an accurate double tangent construction.

VI. DISCUSSION

This paper's method of calculating the high-density free energy from a partition-function product representation, Eq. (9), is a general technique which can be formulated in more than one way. Indeed, de Boer and co-workers[12] have devised a similar scheme, the "cell-cluster theory", which has specifically been applied to rigid disks.[13] This "cell-cluster theory," formulated as it was for the liquid state, considers products of Y factors for arbitrary numbers of independent non-overlapping cell clusters and as such introduces a difficult counting or combinatorial problem which has never been solved exactly even for the two particle cluster term.

However by assigning an arbitrary ordering parameter λ^{n-1} to each cluster involving n particles, the "cell-cluster theory" can be expanded in powers of λ, thus eliminating the difficult combinatorial problem for the first few terms.

The series for the constant C (for $n=1, 2, 3$) can then be alternatively formulated in the following schematic way.

$$C=C_1+C_2+C_3+\cdots,$$

$$C_1=0.14384,$$

$$C_2=-0.01386,$$

$C_3=$ 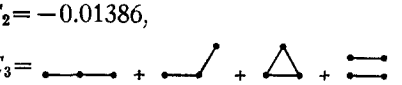

$$=0.014676. \qquad (51)$$

The first two terms are identical to those in Eq. (45). The third term differs by the independent pair term which however makes only a small contribution.

Successive terms from the "cell-cluster theory" will involve increasingly more complicated combinatorial problems arising from the inclusion of several non-overlapping figures. The formulation given in this article, on the other hand, is just as valid in principle and involves, to each order, only connected figures.

Having formulated an algorithm for successive approximations to the free energy there is still an arbitrariness as to how one defines the Z_i, Z_{ij}, etc. For example, one might choose the solution of the Kirkwood free-volume integral equation[14] as the first approximation and formulate analogous integral equations for successive n particle clusters, a procedure too prohibitive to contemplate seriously. For comparison's sake, however, we note that the solution to the single-particle Kirkwood integral equation yields the following value for C:

$$C=1.53013, \qquad (52)$$

a value much larger than the result through fourth order given in Eq. (45).

Another alternative approach that might be employed would be the calculation of free-energy changes for a set of cells with periodic boundary conditions containing ascending numbers of particles. The leading term would then correspond to the correlated cell model introduced by Alder *et al.*[15] which is based on the rectangular two-particle cell in the hexagonal lattice. Introducing corrections due to all rectangular four-particle cells under periodic boundary conditions one obtains

$$C=-0.14384+0.29859+\cdots,$$

$$\cong 0.15475, \qquad (53)$$

including only the two leading terms shown. The first term, from the original correlated cell model has the same magnitude but opposite sign to the cell model we have adopted. The first correction is then large and this series does not appear to be as well behaved as the one in Eq. (45).

Perhaps the most intriguing questions about our general approach concern its application to the three-dimensional rigid-sphere system. Unlike rigid disks, for which the hexagonal lattice arrangement definitely provides the unique closest-packed structure, rigid spheres exhibit stacking degeneracy connected with placing of successive layers of spheres upon one another, the hexagonal and face-centered cubic structures representing the simplest regular stackings. In fact it has not even been established that these "close-packed" arrangements provide the largest obtainable density, though as is customary we assume that they do.

Figure 5 shows the two types of dodecahedral free-volume cells that one sphere experiences at high com-

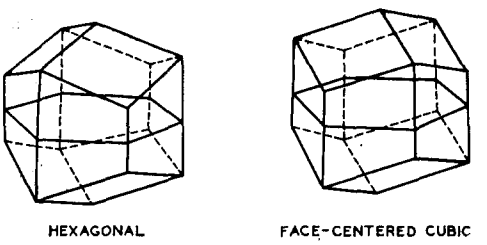

FIG. 5. Free-volume dodecahedra at high compression for the hexagonal and face-centered cubic packings of spheres in three dimensions. The equatorial planes are also shown, to emphasize that these cells are interconvertible by a 60° rotation of one hemisphere.

[12] E. G. D. Cohen, J. de Boer, and Z. W. Salsburg, Physica **21**, 137 (1955).
[13] E. G. D. Cohen and B. C. Rethmeier, Physica **24**, 959 (1958).
[14] J. G. Kirkwood, J. Chem. Phys. **18**, 380 (1950); W. W. Wood, *ibid.* **20**, 1334 (1952).
[15] B. J. Alder, W. G. Hoover, and T. E. Wainwright, Phys. Rev. Letters **11**, 241 (1963).

pression due to the twelve neighbors fixed on a suitable reference lattice. Since one such cell may be transformed into the other type by a 60° rotation of its upper half, the free volumes are the same, and the limiting free energy predicted by our product representation (9) truncated after the single-particle factors would be the same for any of the close-packed lattices, whether layers were placed in regular succession or not. This equivalence of free energies, however, apparently will not persist with inclusion of higher order $Y^{(n,a)}$. Although the particle pair factors for two spheres in the *same* layer may easily be shown to be identical whether the two neighboring layers have caused the dodecahedra to be of the cubic or of the hexagonal types shown in Fig. 5, this need not be the case for two neighboring spheres in *successive* layers. One must therefore expect to find a different high-density free energy for different structures. Similarly the higher order factors in (9) should exhibit structure dependence. Since the thermodynamically stable phase possesses minimum free energy, the approach used in this article constitutes a means of discriminating theoretically between various structures. In this way it should be possible to assert whether or not the high-density phases observed in rigid sphere machine calculations with the relatively small systems used correctly exhibit the infinite system limit structure. We hope to report quantitatively on these matters in a future communication.

ACKNOWLEDGMENTS

F.H.S. wishes to thank Dr. B. J. Alder for discussions on the rigid-disk system, during which the importance of high-density absolute free energy became clear. The authors also wish to thank Mr. David L. Matthews for calling their attention to some of the five particle cluster graphs overlooked in the preliminary manuscript.

APPENDIX

The one-dimensional analog of the rigid-disk system, rigid rods on a line, provides a convenient exactly soluble example for which the additive free-energy constant series is demonstrably convergent. We assume that N rods of length a are confined to a line of length L. Then if these rods are placed at N regularly spaced reference sites, separated by distance L/N, each rod is free to move a total distance $2[(L/N)-a]$ in the single-particle approximation. The resulting free-energy estimate corresponding to Eq. (27) for disks, is readily found to be

$$F/NkT \cong \ln(\lambda/a) - \ln(\theta^{-1}-1) - \ln 2, \qquad \text{(A1)}$$

since $Z_i = 2[(L/N)-a]$. This may be compared with the exact result

$$F/NkT = \ln(\lambda/a) - \ln(\theta^{-1}-1) - 1, \quad \theta = Na/L, \qquad \text{(A2)}$$

which follows from the Tonks equation of state.[16]

There is obviously only one type of connected grouping of n particles in this one-dimensional system, which is the linear uninterrupted sequence. Consequently there is but a single $Y^{(n)}$. Furthermore there are exactly $N-n+1$ such sequences of n possible. For this reason Eq. (30) takes the simple form

$$Q_N(\theta) = \lambda^{-N} \prod_{n=1}^{N} [Y^{(n)}(\theta)]^{N-n+1}. \qquad \text{(A3)}$$

The configuration integrals $Z_{1\cdots n}$ out of which the $Y^{(n)}$ are constructed are elementary,

$$\begin{aligned} Z_{1\cdots n} &= \int_0^{(n+1)[(L/N)-a]} dx_1 \int_0^{(n+1)[(L/N)-a]-x_1} dx_2 \\ &\quad \times \int_0^{(n+1)[(L/N)-a]-x_1-x_2} dx_3 \cdots \\ &\quad \times \int_0^{(n+1)[(L/N)-a]-x_1-\cdots-x_{n-1}} dx_n \\ &= \frac{1}{n!}\left[(n+1)\left(\frac{L}{N}-a\right)\right]^n. \end{aligned} \qquad \text{(A4)}$$

From this result one finds the correlated pair factor to be

$$Y^{(2)} = \tfrac{9}{8}. \qquad \text{(A5)}$$

One may easily show by induction for this simple linear system that when $n \geq 3$,

$$Y^{(n)} = Z_{1\cdots n} Z_{1\cdots n-2} / (Z_{1\cdots n-1})^2. \qquad \text{(A6)}$$

It therefore follows from the last two equations that

$$Y^{(n)} = (n/n-1)[1-(1/n^2)]^n \qquad (n \geq 2). \qquad \text{(A7)}$$

If the expression (A7) is substituted into (A3), logarithms taken, and then N allowed to become very large, the free energy per rod becomes

$$\frac{F}{NkT} = \ln\left(\frac{\lambda}{a}\right) - \ln(\theta^{-1}-1) - \ln 2 - \sum_{n=2}^{\infty} \ln\left[\frac{n}{n-1}\left(1-\frac{1}{n^2}\right)^n\right]. \qquad \text{(A8)}$$

Here the complete infinite series for the additive free-energy constant is exhibited explicitly, and since the terms of the series behave as $1/2n^2$ in magnitude for large n, it clearly converges.

[16] L. Tonks, Phys. Rev. **50**, 955 (1936); E. Helfand, H. L. Frisch, and J. L. Lebowitz, J. Chem. Phys. **34**, 1037 (1961). It is a measure of the misleading simplicity of the rigid-rod system that no terms beyond the additive free-energy constant occur, and that the limiting high density expression is exact for all θ.

The identity of (A2) and (A8) is established by noting

$$\lim_{M\to\infty}\prod_{n=2}^{M}\frac{n}{n-1}\left(1-\frac{1}{n^2}\right)^n=\lim_{M\to\infty}\prod_{n=2}^{M}\frac{(n+1)^n(n-1)^{n-1}}{n^{2n-1}}. \quad \text{(A9)}$$

The factors $(n+1)$ and $(n-1)$ in the numerator will cancel in this product with the previous and the following denominators to leave:

$$\lim_{M\to\infty}\frac{1}{2}\frac{(M+1)^M}{M^M}=\tfrac{1}{2}\lim_{M\to\infty}[1+(1/M)]^M=\tfrac{1}{2}e. \quad \text{(A10)}$$

Insertion of (A10) in (A8) obviously reproduces (A2)

THE JOURNAL OF CHEMICAL PHYSICS VOLUME 43, NUMBER 3 1 AUGUST 1965

Electronic Structure of SrO†

M. KAUFMAN,* L. WHARTON,‡ AND W. KLEMPERER§
Department of Chemistry, Harvard University, Cambridge, Massachusetts

(Received 28 January 1965)

Molecular-beam electric-resonance spectra of SrO are measured in the rf and microwave regions. The microwave transitions are induced with a frequency-broadened klystron, greatly reducing the time needed to search for resonances. Rf-microwave double resonance is used to establish the vibrational assignment of the rf spectra from the known assignment of the microwave spectra. The dipole moment and rotation constant of $^{88}Sr^{16}O$ in the lowest two vibrational states are: $\mu_0=8.900$ D, $\mu_1=8.874$ D, $B_0=0.33688$ cm^{-1}, and $B_1=0.33469$ cm^{-1}. These rotation constants show that this $^1\Sigma$ state is identical with the lower state of three optical-emission systems of SrO. With the aid of a molecular-beam magnetic-deflection experiment, it is shown that this state is almost certainly the ground electronic state of SrO. The evidence indicating triplet ground or low-lying states in SrO and the other alkaline-earth oxides is reviewed, and it is concluded that in no alkaline-earth oxide has a triplet ground state been established. SrO has the largest percent ionic character, μ/er, yet observed for any diatomic molecule. The dipole-moment function $\mu(r)$ of SrO differs considerably from that of BaO and cannot be explained by a model of two polarizable ions. A description of the bonding in the alkaline-earth oxides can be obtained from comparisons of recent SCF calculations on LiF and BeO.

INTRODUCTION

THE study of the molecular structure of the alkaline-earth oxides has been limited by the high vaporization temperatures and ease of reduction of these compounds. In addition, the presence of polymeric species and stable alkaline-earth hydroxides has complicated some experiments. Previous work has primarily been studies of the mass spectra of vapor effusing from high-temperature ovens and of the emission spectra produced when alkaline-earth salts or metals are burned in flames or arcs. This article reports a molecular-beam, electric-resonance investigation of the microwave and radio-frequency spectrum of strontium oxide. In addition, it includes a study of the magnetic properties of thermal beams of SrO and BaO. The purpose of this work is to establish the symmetry of the ground electronic state of SrO, to investigate the existence of low-lying electronic states in SrO and BaO, and to obtain a partial description of the electronic-charge distribution in SrO through measurement of its dipole moment.

Ground-State Symmetry of the Alkaline-Earth Oxides

Figure 1 shows the observed electronic states of the alkaline-earth oxides together with those of C_2, which is isoelectronic to BeO and which has been studied more completely than any of the alkaline-earth oxides. (Observed electronic state here means a state that has been rotationally analyzed.) Listed for each state, following Lagergvist,[1] is the ratio of internuclear distance of the state to that of the lowest state. In contrast to the isoelectronic alkali-metal fluorides, the alkaline-earth oxides show rich band spectra in the visible and ultraviolet.

To date, only singlet systems have been observed in the spectra of the alkaline-earth oxides. From one elementary viewpoint, however, triplet ground states are expected, since the lowest state of the neutral alkaline-earth atom is ^1S while that of oxygen is ^3P. By the Wigner–Witmer rule only $^3\Pi$ or $^3\Sigma$ molecular states can correlate with these atomic products. Singlet states must be formed from excited states of the atoms,

† This work was supported by the U. S. Atomic Energy Commission.
* National Institutes of Health Predoctoral Fellow 1962–1964.
‡ Present address: Department of Chemistry, University of Chicago.
§ Alfred P. Sloane Fellow.

[1] A. Lagerqvist, Arkiv Fysik 8, 83 (1954).